Collision Avoidance by IPMC Actuated Robotic Fish using the Collision Cone Approach

V. Sunkara¹, Z. Ye², A. Chakravarthy³, Z. Chen⁴

Abstract—This paper addresses the problem of collision avoidance by robotic fish that have one caudal and two pectoral fins, all driven by Ionic Polymer-Metal Composite (IPMC) actuators, which are often called artificial muscles. A dynamic model of the robotic fish is developed. A collision cone approach is employed, using which an analytical expression of a nonlinear guidance law that generates the requisite acceleration for collision avoidance is determined. This acceleration vector is converted into fin thrusts that satisfy the constraint that all the thrusts are non-negative. The developed guidance law is tested on an integrated simulation setup comprising the dynamic model of the robotic fish, the dynamics of the IPMC actuator and the relative velocity kinematics of the fish to obstacles in its path, and simulations demonstrate the satisfactory working of the integrated system.

I. INTRODUCTION

The development of autonomous robotic fish that can peform effectively in underwater environments is an active area of research. Development of autonomous robotic fish can pave the way for a wide spectrum of underwater applications such as pollutant source seeking, oil spill monitoring, water quality monitoring, providing tsunami and seaquake warning, surveillance of leakage in underwater oil and gas pipelines, mine reconnaissance, fish survey and behavior study, and underwater search and rescue. For exploration of underwater environments using swarms of such robotic fish, the ability of the robotic fish to achieve collision avoidance is essential for safe deployment. Towards this end, this paper employs a collision cone approach [1],[2],[3] which is a reactive, one-step lookahead method that is particularly suitable for on-line implementation.

In its most fundamental form, the collision cone is defined as the instantaneous set of velocities of an object A that will cause it to lie on a collision course with another moving object B. If the velocity of A lies inside the collision cone, then at that instant, A is on a collision course with B. The equations corresponding to the collision cone are nonlinear and are functions of the shapes of A and B, as well as the relative position and relative velocity. Using the

equations for the collision cone, one can design suitable guidance laws to steer the velocity vector of A out of the collision cone. Conceptually, the collision cone approach is similar to the velocity obstacle approach [4] in that both approaches generate $\operatorname{cone}(s)$ of forbidden velocities. The velocity obstacle approach however is largely restricted to circular agents, while the collision cone approach has been used to determine closed-form representations of collision conditions for objects of entirely arbitrary shapes (both convex and non-convex). The advantage of such exact analytical expressions for collision cones lies in the reduced computational usage, which is of immense value in platforms with limited computational resources. The analytical expressions also serve as an efficient platform for the design, analysis and computation of provably safe trajectories [3].

The guidance laws for collision avoidance are tested by simulations on the dynamic model of a robotic fish that employs ionic polymer-metal composites (IPMCs) as actuators to enable fish locomotion. IPMCs are a class of electroactive polymers (EAPs). EAPs are emerging smart materials that can generate large deformations under electrical stimuli [5]. Due to their similarities to biological muscles, EAPs are often called artificial muscles, and they have different configurations, which can be divided into two categories: dielectric EAPs and ionic EAPs. Dielectric EAPs can generate large forces with large deformations [6], [7], [8]; however, they require high actuation voltages (typically higher than 1 kV), which limits their applications in bio-inspired robotic fish. Ionic polymer-metal composites (IPMCs) are an important category of ionic EAPs. Since IPMCs are soft, lightweight, low-power consuming, and are capable of generating flapping motion, they are ideal artificial muscles for small-scale underwater bio-robots.

To date, several efforts have been devoted toward IPMC-powered underwater robots [9], [10], [11]. For example, Tan et al. developed a robotic fish propelled by an IPMC caudal fin [11], and then Chen et al. developed a speed model for the robotic fish [12]. An IPMC-powered robotic manta ray and cow-nose ray have also been developed [13], [14], [15]. Yang and Chen developed a 2D maneuverable robotic fish actuated by multiple IPMC fins [16]. A dynamic model of robotic fish can be used to have a better sense of system behavior and is also required for control design purposes. Several works have focussed on obtaining such dynamic models [17], [18], [19], [20], [21], [22].

This paper analyzes an integrated model comprising the nonlinear guidance law for collision avoidance, the nonlinear fish dynamics of the 2D maneuverable robotic fish [16], and

¹V. Sunkara is a Doctoral student in the Department of Electrical Engineering and Computer Science, Wichita State University, Wichita, KS, USA. vxsunkara@wichita.edu

²Z. Ye is a Doctoral student in the Department of Electrical Engineering and Computer Science, Wichita State University, Wichita, KS, USA. zxye1@wichita.edu

³A. Chakravarthy is an Assistant Professor in Aerospace Engineering and Electrical Engineering, Wichita State University, Wichita, KS, USA. animesh.chakravarthy@wichita.edu

⁴Z. Chen is an Assistant Professor in the Department of Electrical Engineering and Computer Science, Wichita State University, Wichita, KS, USA. zheng.chen@wichita.edu

the IPMC fin dynamics [12] all integrated in a closed-loop system. Section II discusses the fish dynamic model, the IPMC fin dynamics and the 2D maneuverable robotic fish dynamics. Section III discusses the nonlinear guidance law, the conversion of the acceleration command generated by this guidance law into non-negative fin thrusts, and its integration with the fish dynamic and IPMC actuator model. Section IV presents the simulations of this integrated system, while section V presents the conclusions.

II. ROBOTIC FISH DYNAMIC MODEL

A. Fish Body Dynamics

Refer Figure 1, which shows a schematic of the robotic fish. A body-fixed XY co-ordinate frame is defined such that the X-axis points out the nose of the robotic fish, and the Y-axis is positive towards its left (See Figure 1). The equations of motion of the robotic fish are [21]:

$$\dot{u} = \frac{m_b - m_y}{m_x} vr + \frac{f_x}{m_x} \tag{1}$$

$$\dot{u} = \frac{m_b - m_y}{m_x} vr + \frac{f_x}{m_x}$$

$$\dot{v} = \frac{m_b - m_x}{m_x} ur + \frac{f_y}{m_y}$$
(2)

$$\dot{r} = \frac{\tau_z}{I_z} \tag{3}$$

$$\dot{\psi} = r \tag{4}$$

Here, u and v represent the velocity components along the Xand Y axes, while f_x , f_y represent the respective forces. m_x and m_y are the robot effective masses along the X and Ydirections, respectively, and I_z is the effective inertia about the z axis. ψ represents the heading angle, defined as the angle between the body-fixed XY coordinate frame and an inertial reference frame. r is the angular velocity of the fish body.

When a body moves in a fluid, a portion of the surrounding fluid also moves with the body. This is called the added mass effect. We consider the added mass effect as an additional component m_a added to the body mass m_b . Along similar lines, we also consider the effect of inertia of the surrounding fluid by means of an added-inertia effect. The added mass

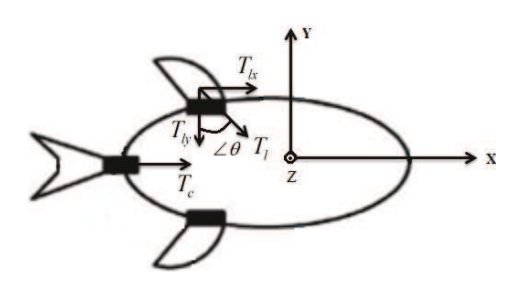


Fig. 1. Robotic fish in body-fixed coordinate axes

 m_{ay} along the y direction and added inertia along the zdirection can be obtained using slender body theory [23]:

$$m_{ay} = \pi \rho R^2 \left(x_2 - x_1 \right) \tag{5}$$

$$I_{az} = \pi \rho R^2 \frac{x_2^3 - x_1^3}{3} \tag{6}$$

where x_1 and x_2 are the pectoral fin locations. For calculating the added mass m_{ax} along the x-direction, we use a procedure which considers the robot body as an ellipsoid of length of l_e and diameter d_e [23]:

$$m_{ax} = \frac{2\pi l_e d_e^2}{6} \tag{7}$$

Finally, m_x , m_y and I_z are obtained as follows:

$$m_x = m_b + m_{ax}; \quad m_y = m_b + m_{ay}; \quad I_z = I_b + I_{az}$$
 (8)

The forces along x and y directions are computed from the thrust and drag forces as follows.

$$f_x = T_c + T_r cos(\theta_P) + T_l cos(\theta_P) - F_D cos(\beta)$$
 (9)

$$f_{y} = T_{r}sin(\theta_{P}) - T_{l}sin(\theta_{P}) - F_{D}sin(\beta)$$
 (10)

$$\tau_z = M_h + M_D \tag{11}$$

In the above equations, T_c is the caudal actuator thrust, T_r and T_l are the right and left pectoral fin thrusts, θ_P is the angle between x axis and right pectoral fin. The two pectoral fins are symmetrically installed. The angle β is defined as $\tan^{-1}(\frac{v}{u})$. M_h is the total hydrodynamic moment and is given by:

$$M_h = \vec{r}_{Cr} \times \vec{T}_r + \vec{r}_{Cl} \times \vec{T}_l \tag{12}$$

Where \vec{r}_{Cr} is the vector from the body center C to the base of the right pectoral fin, and \vec{r}_{Cl} is the corresponding vector to the base of the left pectoral fin. F_D is the drag force, and M_D is the moment due to drag, and these are obtained from the following equations:

$$F_D = \frac{1}{2}\rho U^2 S_A C_D \tag{13}$$

$$M_D = -C_M r^2 sgn(r) (14)$$

where S_A is the robotic fish wetted surface area, C_D is the drag coefficient, U is the speed of the robotic fish, and C_M is the drag moment coefficient.

B. IPMC Fin Dynamics

An IPMC consists of an ion exchange membrane coated with two novel metal electrodes [24], such as gold or platinum. Application of a small voltage to the IPMC leads to ion transportation to the cathode side, which causes a swelling effect on that side and a shrinking effect on the anode side. Eventually, the IPMC bends to the anode side, thus realizing the actuation effect. Chen et. al. obtained the equations governing the thrust generated by an IPMC actuator in water using Lighthill theory of elongated-body [12]. Based on this theory, the mean thrust \overline{T} produced by an IPMC actuator is:

$$\overline{T} = \left[\frac{m}{2} \left(\left(\frac{\partial w(z,t)}{\partial t} \right)^2 - U^2 \overline{\left(\frac{\partial w(z,t)}{\partial z} \right)^2} \right) \right]_{z=L_1}$$
(15)

where w is the actuator bending displacement, U is the fish velocity, $z = L_1$ is the length of the tail, (.) denotes the mean value, and m is the virtual mass density at $z = L_1$ which can be expressed as:

$$m = \frac{1}{4}\pi S_c^2 \rho_w B \tag{16}$$

where S_c is the width of the tail at the end, ρ_w is the water density, and B is a non-dimensional parameter close to 1. In (15), $\frac{\partial w(z,t)}{\partial t}$ is the lateral velocity of the IPMC actuator, and $\frac{\partial w(z,t)}{\partial z}$ is the slope at the tip of the tail $(z=L_1)$. Figure 2 shows a hybrid actuator which comprises the IPMC beam, with a passive fin attached to its tip. When a sinusoidal

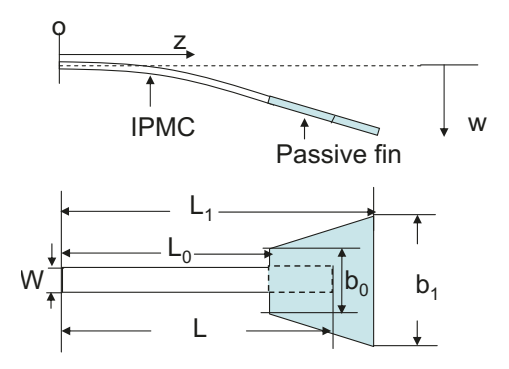


Fig. 2. Illustration of an IPMC beam with passive fin [12].

input voltage is applied to the IPMC, the relevant equations governing the tip displacement and tip slope are [12]:

$$w(L_1, t) = A_m |H(j\omega)| \sin(\omega t + \angle H(j\omega))$$
(17)

$$\frac{\partial w(z,t)}{\partial z}|_{z=L_{1}} = A_{m} |H_{d}(j\omega)| \sin(\omega t + \angle H_{d}(j\omega)) \quad (18)$$

where A_m and ω are the amplitude and frequency of the applied voltage, respectively. $H(j\omega)$ and $H_d(j\omega)$ are the IPMC transfer functions that were derived in [25], and $\angle(.)$ denotes the phase angle. We note that $H(j\omega)$ and $H_d(j\omega)$ are both irrational transfer functions, since the flexible IPMC is modeled as an Euler-Bernoulli beam which is represented by a partial differential equation.

C. Description of the Robotic Fish

Fig. 3 shows an assembled robotic fish [16], whose dimensions and parameters were used for the model simulation and analysis in this paper. In the robotic fish, a microcontroller board (Nano, Arduino) was used to generate three voltage signals applied to the caudal fin and pectoral fins, respectively. A XBee communication device was used to transmit commands from a base station. Three H-Bridges (Gravitech, 2MOTOR-4NANO) were used to amplify the actuation driving current to propel the pectoral and caudal fins. A lithium ion polymer battery (Tenergy, 7.4V 6000 mAh) was used to provide electricity to the robotic fish. The total weight of the robot was 290 grams. Overall, the fish had slightly positive buoyancy. Table I displays the dimensions of the IPMC and the fish body.

III. COLLISION CONE

A. Guidance Law for Collision Avoidance

Refer Figure 4 which shows the robotic fish A and an arbitrarily shaped obstacle B. Let P_1 represent a point on A

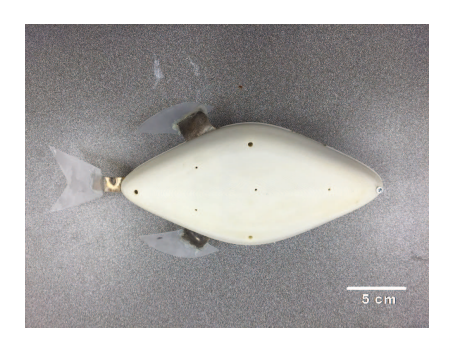


Fig. 3. Assembled robotic fish [16].

TABLE I
SIZE INFORMATION OF IPMC AND FISH BODY

\overline{W}	b_0	b_1	L	L_0	L_1
0.015 m	0.02 m	0.04 m	0.023 m	0.018 m	0.058
x_1	x_2	d_e	l_e	R	θ_P
0.075m	0.157 m	0.05 m	0.23 m	0.08 m	75.3^{o}

(which without loss of generality, can be taken as the center of mass of A), and P_2 represent the corresponding point on B. Then, the kinematic equations of the engagement between the robotic fish and the obstacle are the following:

$$\begin{pmatrix} \dot{\hat{r}} \\ \dot{\hat{\theta}} \\ \dot{\hat{V}}_{\theta} \\ \dot{\hat{V}}_{r} \end{pmatrix} = \begin{pmatrix} \hat{V}_{r} \\ \hat{V}_{\theta}/\hat{r} \\ -\hat{V}_{\theta}\hat{V}_{r}/\hat{r} \\ \hat{V}_{\theta}^{2}/\hat{r} \end{pmatrix} + \begin{bmatrix} 0 \\ 0 \\ -\sin(\delta - \hat{\theta}) \\ -\cos(\delta - \hat{\theta}) \end{bmatrix} a_{A} \quad (19)$$

where \hat{r} , $\hat{\theta}$, represent, respectively, the range and the bearing angle of P_1P_2 . \hat{V}_{θ} , and \hat{V}_r represent, respectively, the relative velocity components normal to, and along, P_1P_2 , a_A is the acceleration of A, applied at an angle δ , as shown in Fig 4.

As demonstrated in [1], two arbitrarily shaped objects are

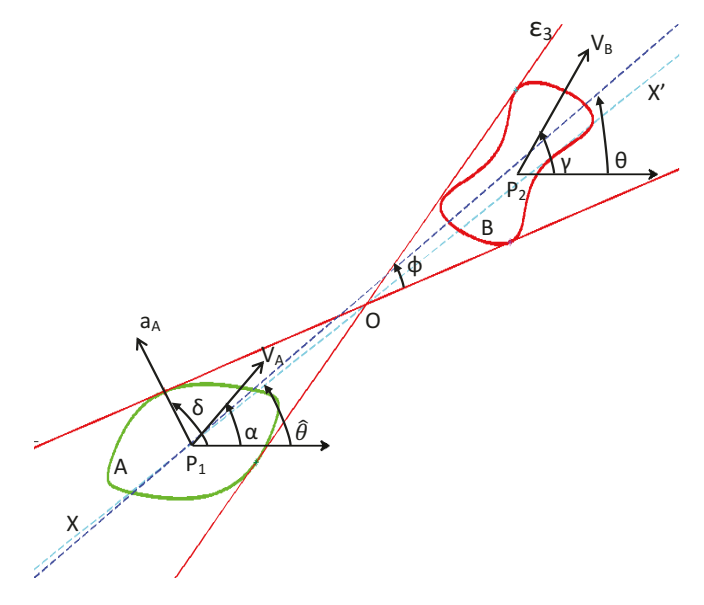


Fig. 4. Engagement geometry between a robotic fish and an obstacle.

on a collision course if their relative velocity components satisfy the conditions: y < 0, $V_r < 0$, where y is defined as follows:

$$y = \csc^2\left(\frac{\phi}{2}\right) \left(\frac{V_\theta^2}{V_\theta^2 + V_r^2}\right) - 1 \tag{20}$$

In (20), ϕ represents the angle of the smallest cone ϵ_3 , that can be formed such that the robot and the obstacle are completely enclosed inside ϵ_3 and lie on opposite sides of its vertex. V_r and V_θ represent the relative velocity components of the angular bisector of ϵ_3 , where V_r is the component along this bisector and V_θ is the component normal to this bisector. The quantites V_r, V_θ are related to $\hat{V}_r, \hat{V}_\theta$ by the relation:

$$\begin{bmatrix} \hat{V}_r \\ \hat{V}_{\theta} \end{bmatrix} = \begin{bmatrix} \cos(\hat{\theta} - \theta) & -\sin(\hat{\theta} - \theta) \\ \sin(\hat{\theta} - \theta) & \cos(\hat{\theta} - \theta) \end{bmatrix} \begin{bmatrix} V_r \\ V_{\theta} \end{bmatrix}$$
(21)

In the special case when A and B are both circular objects, then the angular bisector of ϵ_3 coincides with P_1P_2 , that is, $\hat{\theta} = \theta$, and thus, $V_r = \hat{V}_r$, $V_{\theta} = \hat{V}_{\theta}$.

If the two objects move with constant velocities, then y < 0, $V_r < 0$ are necessary and sufficient conditions for collision to occur. If they move with varying velocities, then y < 0, $V_r < 0$ is a necessary condition for collision to occur. Note that the condition y < 0, $V_r < 0$ physically corresponds to the scenario wherein the relative velocity vector lies inside the collision cone. When y = 0, $V_r < 0$, this physically corresponds to the scenario wherein the relative velocity vector is aligned with the boundary of the collision cone. A sufficient condition for collision avoidance is to ensure that $y \ge 0$ is satisfied at the instant of closest approach.

We determine a guidance law for collision avoidance as follows. Note that the kinematic equation (19) is affine in a_A , and we can use dynamic inversion to determine an analytical guidance law for a_A (applied at an angle δ), that will drive y(t) from an initial negative value to a non-negative reference value. Define an error signal e(t) = w(t) - y(t), where $w(t) \geq 0$ is a reference input. Thus, $\dot{y} = \dot{w} - \dot{e}$. Taking $w(t) = constant \ \forall \ t$ and enforcing the error dynamics to be $\dot{e} = -Ke$, (with K > 0), we get $\dot{y} = K(w - y)$. Using a dynamic inversion technique in conjunction with (20), (19) and (21), we eventually obtain:

$$a_{A} = \left[-K(y-w)(V_{r}^{2} + V_{\theta}^{2})^{2} + 2(V_{r}^{2} + V_{\theta}^{2})\operatorname{cosec}^{2}\frac{\psi}{2} \right]$$

$$V_{\theta}^{2}(V_{r}\dot{\theta}/V_{\theta} + \cot(\frac{\psi}{2})\frac{\dot{\psi}}{2})]/$$

$$\left[2V_{r}V_{\theta}\operatorname{cosec}^{2}\frac{\psi}{2}(-V_{r}\sin(\delta - \theta) + V_{\theta}\cos(\delta - \theta))\right]$$
(22)

Equation (22) is a guidance law that will drive y(t) to $w \ge 0$. Note that since the error dynamics $\dot{e} = -Ke$ are of first order, therefore any positive value of K will guarantee that e(t) decays exponentially to zero. Note also that the above guidance law is a function of δ , which represents the angle at which this acceleration is applied (See Figure 4). If δ is such that the acceleration is applied in the same direction as

the velocity vector of the fish, then a_A is a pure translational acceleration and the fish experiences a change in speed with no change in its velocity heading angle. If δ is such that the acceleration is applied normal to the velocity vector of the fish, then a_A results in a pure lateral acceleration, which causes the velocity vector of the fish to rotate (that is, causes a change in heading angle) while the speed of the fish remains constant. If δ is applied at any other angle, then the effect of a_A is a combination of speed and heading angle change.

B. Conversion of commanded acceleration into fin thrusts

The acceleration generated by (22) now needs to be converted into thrusts T_c (of the caudal fin), and T_l , T_r (of the left and right pectoral fins). Collision avoidance of the fish with the obstacle can be achieved in one of three different ways:

- (a) Generate an appropriate moment using the pectoral fin thrusts to create a turning trajectory for the fish to move around the obstacle. The value of this moment is given by $M_h = K a_A$, where K is an appropriate proportional gain, a_A is the acceleration generated by (22), applied at an angle $\delta = \alpha + \frac{\pi}{2}$. Depending on whether M_h needs to be clockwise or counter-clockwise, only one of T_l or T_r are non-zero. The corresponding T_l (or T_r) is determined using (12).
- (b) Perform a pure translational acceleration using just the caudal fin alone, i.e., $T_c > 0$, while keeping the pectoral fin thrusts zero, i.e., $T_l = 0, T_r = 0$. This essentially involves a pure speed change maneuver performed by the fish, while keeping the direction of its velocity vector constant.
- (c) Generate an appropriate combination of lateral and translational acceleration components, with $T_c>0$, and either (i) $T_l>0$, $T_r=0$, or (ii) $T_l=0$, $T_r>0$. This essentially involves the fish generating a component of sideways motion in order to bypass the obstacle.

We point out that if we use (c) then, along with the sideways motion component generated by the corresponding pectoral fin thruster, a turning component is also generated. Similarly, if we use (a) then, along with the turning moment, a sideways motion component is also generated. The choice of which method to use depends on the location of the pectoral fins relative to the center of gravity of the fish. If the pectoral fins are so located that they generate relatively small turning moment, then one would prefer to use method (c), while if they are so located that they generate a large turning moment, then we would prefer to use (a).

Now, since T_c , T_l , and T_r need to be non-negative at all times, this imposes a constraint on the (a_A, δ) pairs that can be used to achieve collision avoidance, at each instant in time. In other words, when $y < 0, V_r < 0$, (a_A, δ) need to satisfy not just the acceleration equation (22) for collision avoidance, but also the constraints $T_c \ge 0$, $T_l \ge 0$, $T_r \ge 0$. For case (a), the thrusts are always positive, while for case (b) one can ensure that the thrusts are positive simply by choosing the angle $\delta = \psi$.

For case (c), more analysis is required. From (9), (10), the

thrust equations can be written as:

$$T_c + T_l \cos \theta_P + T_r \cos \theta_P = y_1 \tag{23}$$

$$T_r \sin \theta_P - T_l \sin \theta_P = y_2 \tag{24}$$

where,

$$y_1 = m_x a_A \cos(\delta - \psi) + F_D \cos \beta \tag{25}$$

$$y_2 = m_y a_A \sin(\delta - \psi) + F_D \sin \beta \tag{26}$$

From (24)-(26), we see that in order to obtain positive thrusts $T_l > 0$ and $T_c > 0$, we need to satisfy the following two inequalities:

$$y_2 < 0 \tag{27}$$

$$y_1 + y_2 \cot \theta_P > 0 \tag{28}$$

We now look for a range of (a_A,δ) pairs that satisfy both inequalities. Defining $q=\frac{-F_Dsin\beta}{a_Am_y}$, we see that (27) can be satisfied as follows:

Case (1): When $a_A > 0$, and

(a) $\beta \in (\pi, 2\pi)$: We need that $\delta \in R_{1a}$, where

$$R_{1a} = \{ \delta : \delta \in (0, \psi + \sin^{-1} q) \cup (\pi - \sin^{-1} q + \psi, 2\pi) \}$$

(b) $\beta \in (0,\pi)$: We need that $\delta \in R_{1b}$, where

$$R_{1b} = \{\delta : \delta \in (\sin^{-1} q + \psi, 2\pi - \sin^{-1} q + \psi)\}$$
 (30)

Case (2): When $a_A < 0$, and

(a) $\beta \in (0,\pi)$: We need that $\delta \in R_{2a}$, where

$$R_{2a} = \{\delta : \delta \in (\psi + \sin^{-1} q, \pi + \psi - \sin^{-1} q)\}$$
 (31)

(b) $\beta \in (\pi, 2\pi)$: We ned that $\delta \in R_{2b}$, where

$$R_{2b} = \{ \delta : \delta \in (\psi, \pi + \sin^{-1} q + \psi) \cup (2\pi - \sin^{-1} q + \psi, 2\pi + \psi) \}$$
(32)

Next, considering the inequality (28), this can be rewritten in the quadratic form $a_0Z^2 + a_1Z + a_2 > 0$, where $Z = \tan(\delta/2)$ and

$$a_0 = -a_A m_x \cos(\psi) + F_D \cos(\beta) + a_A m_y \cot(\theta) \sin(\psi)$$

$$+ F_D \sin(\beta) \tag{33}$$

$$a_1 = 2a_A m_x \sin(\psi) + 2a_A m_y \cot(\theta) \cos(\psi) \tag{34}$$

$$a_2 = F_D \cos(\beta) - a_A m_x \cos(\psi) - a_A m_y \cot(\theta) \sin(\psi)$$

$$+ F_D \sin(\beta) \cot(\theta) \tag{35}$$

Defining the roots of the quadratic equation as $Z_{1,2}$, where

$$Z_{1,2} = \frac{-a_1 \pm \sqrt{a_1^2 - 4a_0 a_2}}{2a_0} \tag{36}$$

the possible cases then are:

Case (3): When $a_0 > 0$, (28) is satisfied when $\delta \in R_{3a} \cup R_{3b}$, where:

$$R_{3a} = \{\delta : \delta \in (2\tan^{-1} Z_1, \pi)\}$$
 (37)

$$R_{3b} = \{\delta : \delta \in (-\pi, 2\tan^{-1} Z_2)\}$$
 (38)

Case (4): When $a_0 < 0$, (28) is satisfied when $\delta \in R_{4a} \cup R_{4b}$,

where:

$$R_{4a} = \{\delta : \delta \in (2\tan^{-1} Z_2, \pi)\}$$
 (39)

$$R_{4b} = \{\delta : \delta\epsilon \left(-\pi, 2\tan^{-1} Z_2\right)\} \tag{40}$$

Combining all of the above cases, we need the following in order to satisfy the two inqualities (27), (28) simultaneously:

$a_A > 0, \ \beta \in (\pi, 2\pi), \ a_0 > 0$	$\delta \in R_{1a} \cap \{R_{3a} \cup R_{3b}\}$
$a_A > 0, \ \beta \in (\pi, 2\pi), \ a_0 < 0$	$\delta \in R_{1a} \cap \{R_{4a} \cup R_{4b}\}$
$a_A > 0, \ \beta \in (0, \pi), \ a_0 > 0$	$\delta \in R_{1b} \cap \{R_{3a} \cup R_{3b}\}$
$a_A > 0, \ \beta \in (0, \pi), \ a_0 < 0$	$\delta \in R_{1b} \cap \{R_{4a} \cup R_{4b}\}$
$a_A < 0, \ \beta \in (0, \pi), \ a_0 > 0$	$\delta \in R_{2a} \cap \{R_{3a} \cup R_{3b}\}$
$a_A < 0, \ \beta \in (0, \pi), \ a_0 < 0$	$\delta \in R_{2a} \cap \{R_{4a} \cup R_{4b}\}$
$a_A < 0, \ \beta \in (\pi, 2\pi), \ a_0 > 0$	$\delta \in R_{2b} \cap \{R_{3a} \cup R_{3b}\}$
$a_A < 0, \ \beta \in (\pi, 2\pi), \ a_0 < 0$	$\delta \in R_{2b} \cap \{R_{4a} \cup R_{4b}\}$

At each instant in time, the appropriate (a_A, δ) pair that satisfies (22) and the relevant condition in the above table is chosen. A corresponding set of equations can be determined when the fish needs to pass the obstacle on the left of the obstacle, with $T_r > 0$, $T_l = 0$.

C. Integrated system architecture

A block diagram of the overall integrated system is shown in Fig 5. The guidance law acceleration a_A generated from (22) is converted into reference thrust commands $T_{c,R}$, $T_{l,R}$, and $T_{r,R}$ of the caudal, left and right pectoral fins, while ensuring that all these thrusts are non-negative using the equations described above. These reference thrusts are then converted into amplitudes $A_{m,c}$, $A_{m,l}$ and $A_{m,r}$ of sinusoidal voltages of the three IPMC actuators, using:

$$A_{m,c} = \sqrt{\frac{4T_{c,R}}{m(\omega^2|H|^2 - U^2|H_d|)^2}}$$
(41)

$$A_{m,l} = \sqrt{\frac{4T_{l,R}}{m(\omega^2|H|^2 - U^2|H_d|)^2}}$$
 (42)

$$A_{m,r} = \sqrt{\frac{4T_{r,R}}{m(|\omega^2|H|^2 - U^2|H_d|)^2}}$$
 (43)

where ω is the frequency of the sinusoidal voltage, and H, H_d are IPMC transfer functions, derived in [25]. The IPMC actuators then convert these voltage inputs into actual thrusts \overline{T}_c , \overline{T}_l , and \overline{T}_r , using (15), where the tip deflection and tip slope are computed using (17) and (18), respectively. These thrusts influence the robot fish dynamics (1)-(4). The movement of the robotic fish, along with the movements of the obstacle, influence the relative velocity kinematic states \hat{r} , $\hat{\theta}$, \hat{V}_{θ} , and \hat{V}_r , shown in (19). These in turn influence the quantity y used in the collision cone computations, and shown in (20). The value y along with the relative kinematic states is then fed back towards computation of the guidance law acceleration a_A .

IV. SIMULATION RESULTS

In this section, we demonstrate simulation results corresponding to the integrated system depicted in the block diagram shown in Figure 5. The shape of the fish is defined

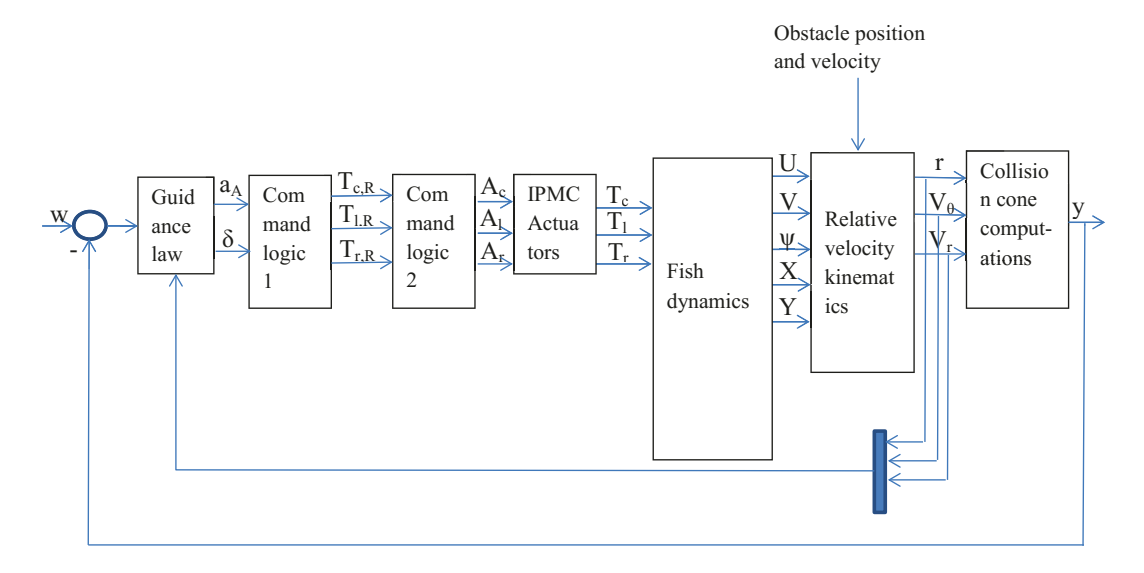


Fig. 5. Block diagram depicting the integration of the guidance law with the IPMC actuator and fish dynamics.

by the equation:

$$X = R_x \cos(\theta_R)$$

$$Y = R_y \sin(\theta_R) - K_R R_y \sin^3(\theta_R)$$
 (44)

where $R_x=0.3\,$ m, $R_y=0.1\,$ m, $K_R=-1$, for the host fish A, and $R_x = 0.2 \ m, \ R_y = 0.2 \ m, \ K_R = -0.5$ for the two obstacle fish B & C, with θ_R varying from 0^o to 360^o . Note that the equation of the fish shape corresponds to the fish depicted in Figure 3. The initial position of the fish is taken to be at the origin of an inertial frame, and its velocity is 2 cm/sec, with a velocity heading angle of 45 deg. Two obstacle fish B and C, are assumed. The initial position of B is (3 m, 6.1 m), and its velocity is 2 cm/sec. The obstacle fish C appears at 240 sec, at a location of (6 m, 5 m), moving with a velocity of 0.15 cm/sec. We note that these speed values reflect numbers that are in line with what IPMC actuators are capable of producing. From Figures 6) and 7, it is evident that y(0) < 0 which in conjunction with $V_r(0) < 0$ indicates a situation wherein the initial velocity vector of A lies inside the collision cone to B.

As can be seen from Figure 7, the initial negative value of y is driven to w=0.2 around t=140 sec, by application of a turning moment that is proportional to the lateral acceleration. The relative velocity kinematics are shown in Figure 6, and the time history of the angle ϕ used to compute the lateral acceleration is shown in Figure 11(c). The evolution of the angle δ at which the acceleration is applied, is shown in Figure 7(c). The acceleration is converted into thrust commands of the caudal fin (shown in Figure 8(a)) and the left pectoral fin (shown in Figure 9(a)).

The thrust commands are then converted into amplitudes of the sinusoidal voltage applied to the IPMC actuator. These voltages are shown in Figure 8(b) (for the caudal fin), and Figure 9(b) (for the left pectoral fin). The ensuing tip deflections and tip slopes for each of the IPMC actuators are shown in Figure 8(c),(d) and 9(c),(d). Note that these plots

show the amplitude of the underlying sine wave trajectories (shown as an inset in these figures) of the tip deflection and slope. The tip deflections are of the order of 10 cm, while the tip slopes are of the order of 0.5 rad, which are reasonable values corresponding to the IPMC actuator. During t =[140,240] sec, the collision avoidance acceleration drops to zero, and accordingly so does the left pectoral thrust. The second fish C appears at t = 240 sec, and this fish also lies in the collision cone of A (as evident from Figures 6 and 7). To avoid fish C, fish A again executes a turning motion, this time using a moment generated by the right pectoral fin, while the thrust from the left pectoral fin is zero. The relevant plots of the thrust, voltage amplitude, and amplitudes of the tip deflection and tip slope of the right pectoral fin are shown in Figure 10. Figure 12 shows the spatial trajectories of the robotic fish A and the other two fish B and C.

V. CONCLUSIONS

This paper addresses the problem of collision avoidance of IPMC-actuated robotic fish (with one caudal and two pectoral fins) using the collision cone approach. The collision cone approach allows a closed form determination of analytical conditions for collision avoidance for arbitrary objects moving on a plane. An analytical guidance law for collision avoidance is determined, and this law is used to compute both the acceleration magnitude and direction in an appropriate fashion so as to result in non-negative reference thrusts of the caudal and pectoral fins of the fish. These reference thrusts are then converted into sinusoidal voltages of the IPMC actuators, which drive the three fins. Simulations are performed to characterize the complete closed loop system incorporating the nonlinear collision cone-based guidance law, the irrational transfer function corresponding to the IPMC actuators and the nonlinear dynamics of the robotic fish, and these demonstrate satisfactory performance of the integrated system.

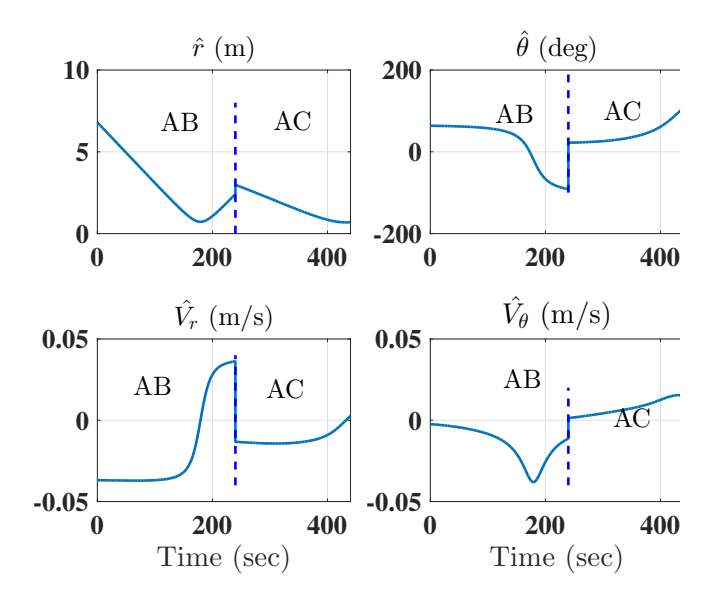


Fig. 6. Kinematic state trajectories of engagement between the robotic fish A and obstacle fish B & C: (a) \hat{r} , (b) $\hat{\theta}$, (c) \hat{V}_{θ} , (d) \hat{V}_{r} .

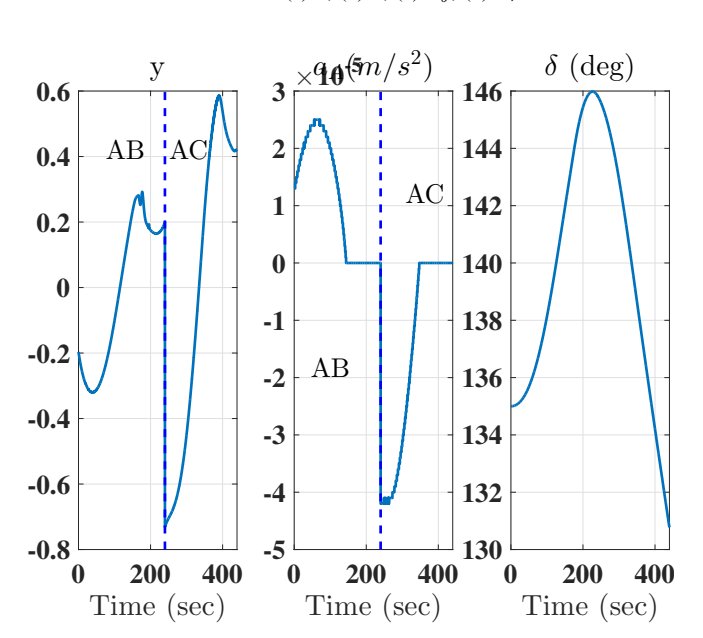


Fig. 7. (a) Output y of robotic fish A to fish B & C, (b) Commanded acceleration a_A by collision avoidance law, (c) δ .

VI. ACKNOWLEDGEMENTS

This work is supported by the National Science Foundation under Grants IIS-1351677 and CNS-1446557.

REFERENCES

- [1] A. Chakravarthy and D. Ghose, "Obstacle avoidance in a dynamic environment: a collision cone approach," *IEEE Transactions on Systems, Man and Cybernetics Part A:Systems and Humans*, vol. 28, pp. 562–574, 1998.
- [2] —, "Collision cones for quadric surfaces," *IEEE Transactions on Robotics*, vol. 27, pp. 1159–1166, 2011.
- [3] —, "Generalization of the collision cone approach for motion safety in 3-d environments," *Autonomous Robots*, vol. 32, pp. 243–266, 2012.
- [4] P. Fiorini and Z. Shiller, "Motion planning in dynamic environments using velocity obstacles," *International Journal of Robotics Research*, 1998.

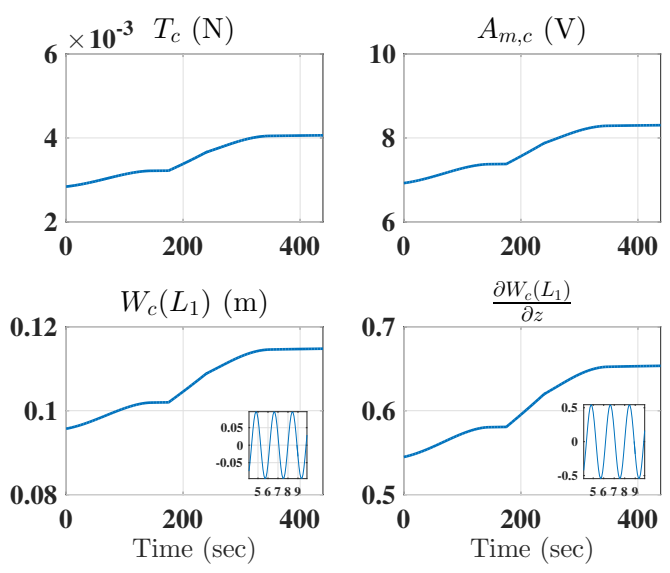


Fig. 8. (a) Caudal Thrust, (b) Voltage Amplitude, (c) Tip deflection amplitude, (d) Tip slope amplitude of IPMC Actuator of caudal fin.

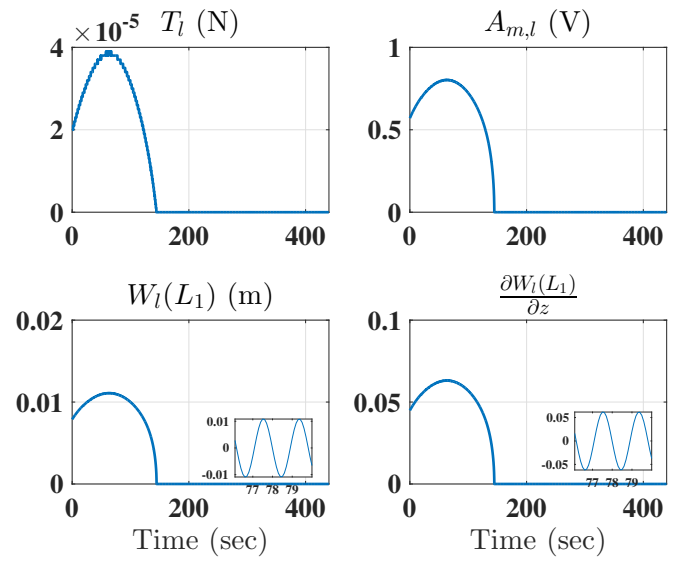


Fig. 9. (a) Left Pectoral Thrust, (b) Voltage Amplitude, (c) Tip deflection amplitude, (d) Tip slope amplitude of IPMC Actuator of left pectoral fin.

- [5] Y. Bar-Cohen, Electroactive polymers as artificial muscles: Capabilities, potentials and challenges in Handbook on Biomimetics, Y. Osada, Ed. Ed. NTS Inc., 2000.
- [6] R. Pelrine, R. Kornbluh, Q. Pei, and J. Joseph, "High-speed electrically actuated elastomers with strain greater than 100287, no. 5454, pp. 836–839, Feb. 2000.
- [7] Z. Suo, "Theory of dielectric elastomers," Acta Mechanica Solida Sinica, vol. 23, pp. 549–578, 2010.
- [8] F. Carpi, D. D. Rossi, R. Kornbluh, R. Pelrine, and P. Sommer-Larsen, "Dielectric elastomers as electromechanical transducers," *Elsevier*, 2008
- [9] S. Guo, T. Fukuda, and K. Asaka, "A new type of fish-like underwater microrobot," *IEEE/ASME Transactions on Mechatronics*, vol. 8, no. 1, pp. 136–141, 2003.
- [10] H. Hu, J. Liu, I. Dukes, and G. Francis, "Design of 3d swim patterns for autonomous robotic fish," in *Proceedings of the 2006 IEEE/RSJ International Conference on Intelligent Robots and Systems, Beijing, China*, 2006, pp. 2406–2411.

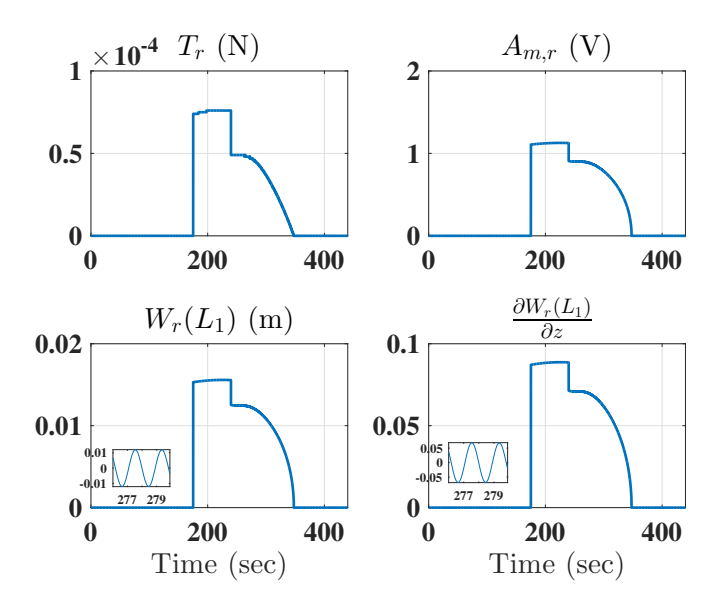


Fig. 10. (a) Right Pectoral Thrust, (b) Voltage Amplitude, (c) Tip deflection amplitude, (d) Tip slope amplitude of IPMC Actuator of right pectoral fin.

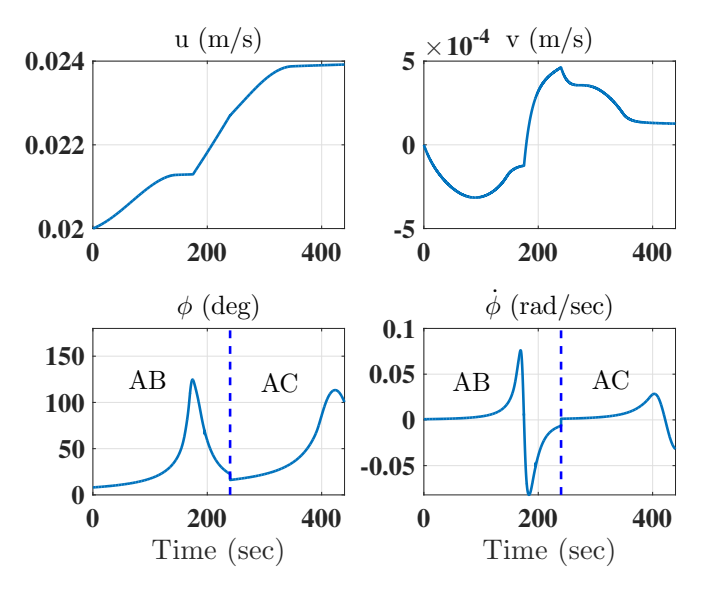


Fig. 11. (a)-(b) Body axis velocity components, u and v of robotic fish, (c) Time history of angle ϕ between robotic fish A and B & C, (d) Time history of $\dot{\phi}$ between robotic fish A and B & C.

- [11] X. Tan, D. Kim, N. Usher, D. Laboy, J. Jackson, A. Kapetanovic, J. Rapai, B. Sabadus, and X. Zhou, "An autonomous robotic fish for mobile sensing," in *Proceedings of the IEEE/RSJ International Conference on Intelligent Robots and Systems, Beijing, China*, 2006, pp. 5424–5429.
- [12] Z. Chen and X.Tan, "Modeling of biomimetic robotic fish propelled by an ionic polymercmetal composite caudal fin," *IEEE/ASME Trans*actions on mechatronics, vol. 15, no. 3, pp. 448–459, Jun. 2010.
- [13] A. Punning, M. Anton, M. Kruusmaa, and A. Aabloo, "A biologically inspired ray-like underwater robot with electroactive polymer pectoral fins," in *Proceedings of the 2004 IEEE International Conference on Mechatronics and Robotics, Aachen, Germany*, 2004, pp. 241–245.
- [14] Z. Chen, T. Um, J. Zhu, and H. Bart-Smith, "Bio-inspired robotic cownose ray propelled by electroactive polymer pectoral fin," in Proceedings of the ASME 2011 International Mechanical Engineering Congress & Exposition, 2011, p. 797637X.
- [15] Z. Chen, T. Um, and H. Bart-Smith, "Bio-inspired robotic manta

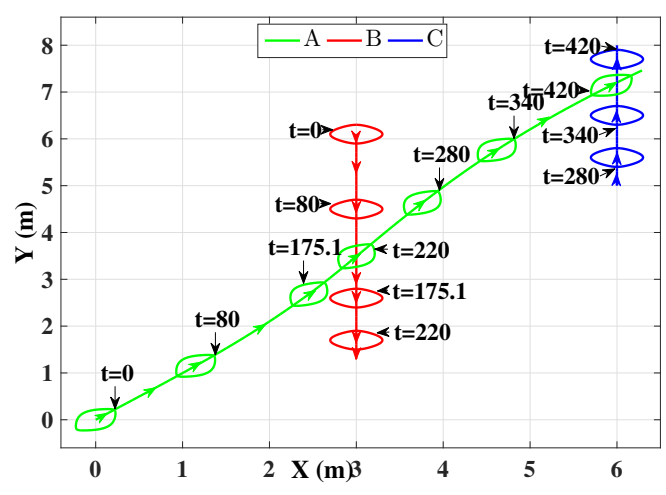


Fig. 12. XY trajectory of robotic fish and obstacle.

- ray powered by ionic polymer-metal composite artificial muscles," *International Journal of Smart and Nano Materials*, vol. 3, pp. 296–308, 2012.
- [16] T. Yang and Z. Chen, "Development of 2d maneuverable robotic fish propelled by multiple ionic polymer-metal composite artificial fins," *Proceedings of the 2015 IEEE Conference on Robotics and Biomimetics*, pp. 255–260, Dec. 2015.
- [17] J. Guo, "A waypoint-tracking controller for a biomimetic autonomous underwater vehicle," *Ocean Eng.*, vol. 33, no. 17-18, pp. 2369–2380, 2006.
- [18] J. Shao, L. Wang, and J. Yu, "Development of an artificial fish-like robot and its application in cooperative transportation," *Control Eng. Practice*, vol. 16, no. 5, pp. 569–584, 2008.
- [19] J. Yu, M. Tan, S. Wang, and E. Chen, "Development of a biomimetic robotic fish and its control algorithm," *IEEE Transactions on Systems, Man, and Cybernetics, Part B (Cybernetics)*, vol. 34, no. 4, pp. 1798– 1810, Aug. 2004.
- [20] J. Wang and X. Tan, "A dynamic model for tail-actuated robotic fish with drag coefficient adaptation," *Mechatronics*, vol. 23, pp. 659–668, 2013
- [21] J. Wang, P. McKinley, and X. Tan, "Dynamic modeling of robotic fish with a base-actuated flexible tail," *Journal of dynamic systems,* measurement, and control, vol. 137, Jan. 2015.
- [22] V. Kopman, J. Laut, F. Acquaviva, A. Rizzo, and M. Porfiri, "Dynamic modeling of a robotic fish propelled by a compliant tail," *IEEE Journal* of oceanic engineering, vol. 40, no. 1, Jan. 2015.
- [23] G. V. Lauder, P. G. A. Madden, J. L. Tangorra, E. Anderson, and T. V. Baker, "Bio-inspiration from fish for smart material design and function," *Smart Materials and Structures*, vol. 20, p. 094014, 2011.
- [24] M. Shahinpoor and K. Kim, "Ionic polymer-metal composites: I. fundamentals," Smart Materials and Structures, vol. 10, pp. 819–833, 2001
- [25] C. Zhou and K. H. Low, "Design and locomotion control of a biomimetic underwater vehicle with fin propulsion," *IEEE/ASME Transactions on Mechatronics*, vol. 17, pp. 25–35, 2012.